Ortho-Hydroxylation of aromatic acids by a non-heme FeVO species: How important is the ligand design?

ARTICLE *in* PHYSICAL CHEMISTRY CHEMICAL PHYSICS · JUNE 2014

Impact Factor: 4.49 · DOI: 10.1039/C3CP55430A

2 AUTHORS, INCLUDING:

Azaj Ansari
Indian Institute of Technology Bombay
8 PUBLICATIONS **38** CITATIONS

PCCP

PAPER

View Article Online
View Journal | View Issue

ortho-Hydroxylation of aromatic acids by a non-heme Fe^{V}=O species: how important is the ligand design?†

Cite this: *Phys. Chem. Chem. Phys.*, 2014, **16**, 14601

Azaj Ansari and Gopalan Rajaraman*

There is a growing interest in probing the mechanism of catalytic transformations effected by non-heme iron-oxo complexes as these reactions set a platform for understanding the relevant enzymatic reactions. The *ortho*-hydroxylation of aromatic compounds is one such reaction catalysed by iron-oxo complexes. Experimentally $[Fe^{II}(BPMEN)(CH_3CN)_2]^{2+}$ (**1**) and $[Fe^{II}(TPA)(CH_3CN)_2]^{2+}$ (**2**) (where TPA = tris(2-pyridylmethyl)amine and BPMEN = *N*,*N*′-dimethyl-*N*,*N*′-bis(2-pyridylmethyl)ethane-1,2-diamine) complexes containing amino pyridine ligands along with H_2O_2 are employed to carry out these transformations where complex **1** is found to be more reactive than complex **2**. Herein, using density functional methods employing B3LYP and dispersion corrected B3LYP (B3LYP-D) functionals, we have explored the mechanism of this reaction to reason out the importance of ligand design in fine-tuning the reactivity of such catalytic transformations. Dispersion corrected B3LYP is found to be superior to B3LYP in predicting the correct ground state of these species and also yields lower barrier heights than the B3LYP functional. Starting the reaction from the Fe^{III}–OOH species, both homolytic and heterolytic cleavage of the O···O bond is explored leading to the formation of the transient Fe^{IV}=O and Fe^{V}=O species. For both the ligand systems, heterolytic cleavage was energetically preferable and our calculations suggest that both the reactions are catalyzed by an elusive high-valent Fe^{V}=O species. The Fe^{V}=O species undergoes the reaction *via* an electrophilic attack of the benzene ring to effect the *ortho*-hydroxylation reaction. The reactivity pattern observed for **1** and **2** are reflected in the computed barrier heights for the *ortho*-hydroxylation reaction. Electronic structure analysis reveals that the difference in reactivity between the ligand architectures described in complex **1** and **2** arise due to orientation of the pyridine ring(s) parallel or perpendicular to the Fe^{V}=O bond. The parallel orientation of the pyridine ring is found to mix with the $(\pi_{Fe(dyz)-O(py)})^*$ orbital of the Fe-oxo bond leading to a reduction in the electrophilicity of the ferryl oxygen atom. Our calculations highlight the importance of ligand design in this chemistry and suggest that this concept can be used to (i) stabilize high-valent intermediates which can be trapped and thoroughly characterized (ii) enhance the reactivity and efficiency of the oxidants by increasing the electrophilicity of the ferryl oxygen containing Fe^{V}=O species. Our computed results are in general agreement with the experimental results.

Received 24th December 2013,
Accepted 14th March 2014

DOI: 10.1039/c3cp55430a

www.rsc.org/pccp

1 Introduction

Selective aromatic hydroxylation is an important reaction in the pharmaceutical industry.[1,2] Hydroxylation reactions are generally catalyzed by mononuclear and dinuclear heme and non-heme iron complexes.[3–14] Naturally, hydroxylations are catalyzed by several non-heme iron enzymes of which some possess one iron centre such as pterin-dependent aromatic amino acid and some possess dinuclear iron sites such as bacterial multi-component methane and toluene monooxygenases.[7–10] Synthetically feasible aromatic hydroxylations have also been reported with iron using Fenton's reagent, however these reactions are non selective due to the generation of hydroxyl radicals.[15–17] Thus the development of stereo and regio-selective catalytic oxidation of organic substrates by non-heme metal complexes is an important reaction that both the organic and the bioinorganic community are vigorously studying over the past decade.[18–20] Biomimetic approaches are particularly attractive as they involve cheap, non-toxic reactants (usually, O_2 or H_2O_2 as oxidants, and Fe, Cu, or Mn complexes as catalysts).[18–21] Due to these reasons, interests in the

Department of Chemistry, Indian Institute of Technology-Bombay, Powai, Mumbai, India. E-mail: rajaraman@chem.iitb.ac.in; Fax: +91-22-2572-3480; Tel: +91-22-2576-7183

† Electronic supplementary information (ESI) available. See DOI: 10.1039/c3cp55430a

synthesis of novel iron complexes possessing the necessary structural flexibilities are targeted to carry out these transformations. Over the years several metal complexes particularly that of iron have been reported for regio-selective hydroxylation and other catalytic transformations.[21,22]

High-valent iron-oxo species are proposed as key intermediates in the heme as well as non-heme iron enzymes.[23–37] Electrophilic attack by the high-valent iron oxo rather than C–H activation is proposed as the key mechanism for the *ortho*-hydroxylation and this is supported by both experiments and our earlier theoretical studies.[38–44] The nature of the species involved is very much debatable, with several aliphatic and aromatic hydroxylation reactions proposed to be catalysed by high-valent Fe^{IV}═O species[45–67] and in some instances they are also characterized by spectroscopic methods.[18,68–89] Besides the Fe^{IV}═O species, the Fe^{V}═O species are also proposed as a potential oxidant in this chemistry and this proposal has gained momentum since the unambiguous chemical and spectroscopic detection of these species with TPP (*meso*-tetraphenylporphinato dianion), ^{Me,H}Pytacn(=1-(2′-pyridylmethyl)-4,7-dimethyl-1,4,7-triazacyclononane)[90] and TAML (tetraamido macrocyclic)[91] ligands. The Fe^{V}═O species containing aminopyridine ligands such as TPA, BPMEN and TMC (tetraazamacrocyclic) are also suggested for the epoxidation and hydroxylation reactions of aliphatic and aromatic compounds.[21,22,92–95] Among the ligand architectures available, tetradentate aminopyridine ligands like the one discussed above are found to be one of the successful ligands for yielding highly selective epoxidation, hydroxylation and C–H activation reactions with hydrogen peroxide as the oxidant.[94,96–100]

Elucidating the mechanism of such reactions holds the key to the development of novel biomimetic model compounds whose reactivity will either be superior or on a par with that of the enzymes. Over the past decades, the mechanism of iron-promoted *ortho*-hydroxylation reaction became a topic of current research in the bioinorganic chemistry community.[68] Recently Que *et al.* reported selective *ortho*-hydroxylation of benzoic acid in the presence of various types of aminopyridine containing iron complexes.[21,22,44] Biomimetic catalysts such as $[Fe^{II}(BPMEN)(CH_3CN)_2]^{2+}$ complex (**1**) and $[Fe^{II}(TPA)(CH_3CN)_2]^{2+}$ (**2**) have been widely studied by experimentalists to probe mechanistic aspects and to elucidate the nature of the oxidant in this chemistry. Complex **1** catalyses the *ortho*-hydroxylation reactions of benzoic acid yielding salicylic acid as the product. Some substituted benzoic acid derivatives on the other hand are found to yield *ipso*-hydroxylated products as well.[21,22] The regiospecificity of these reactions indicates that inner sphere aromatic hydroxylation at the non-heme iron centre is taking place in this reaction. The ^{18}O labelling experiments indicate that one of the oxygens in the product formation is coming from the labelled H_2O_2. Que *et al.* suggest the Fe^{III}–OOH species as the starting point in the mechanistic cycle as this has been detected by spectroscopic methods. This species, during the course of the reaction, can possibly generate either an Fe^{IV}═O or an Fe^{V}═O species by homolytic or heterolytic cleavage of the O···O bond.[22,101,102] Homolytic cleavage of the O···O bond generates hydroxyl radical and this may appear to discourage selectivity, however for pentadentate ligand systems, a caged radical species was suggested to activate this reaction selectively.[103]

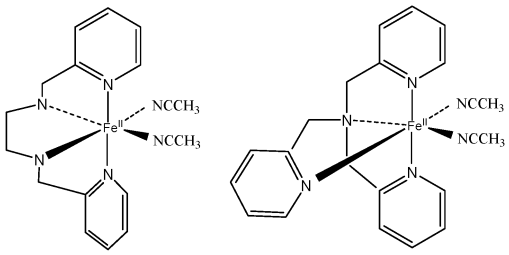

Scheme 1 Schematic diagram of $[Fe^{II}(BPMEN)(CH_3CN)_2]^{2+}$ (complex **1**, left) and $[Fe^{II}(TPA)(CH_3CN)_2]^{2+}$ (complex **2**, right).

Que *et al.* and Rybak-Akimova *et al.* independently reported that the $[Fe^{II}(BPMEN)(CH_3CN)_2]^{2+}$ complex (**1**) is more reactive than the $[Fe^{II}(TPA)(CH_3CN)_2]^{2+}$complex (**2**) (see Scheme 1).[21,22,95] The $[Fe^{II}(BPMEN)(CH_3CN)_2]^{2+}$ complex is one of the best known examples for the hydroxylation reaction.[95] Since both the ligand structures are similar (see Scheme 1), we aim to model the reaction with the Fe–BPMEN ligand system and compare the computed result to that of the TPA system[94] to gain insight into the importance of ligand design in this chemistry. Important questions which we aim to address here are (i) why $[(BPMEN)(PhCOOH)Fe^{V}═O]^{2+}$ is a stronger oxidant than $[(TPA)(PhCOOH)Fe^{V}═O]^{2+}$ species? (ii) And are there any mechanistic differences in the *ortho*-hydroxylation between these two ligand architectures? By answering these two questions, we aim to address the importance of ligand design in enhancing the selectivity and the robustness of the catalytic transformations performed by these transient species.

2 Computational details

All calculations were performed using Gaussian 09 suite of programs.[104] In our earlier work on benchmarking (employing B3LYP,[105,106] B3LYP-D,[107] wB97XD,[108] B97D,[107] M06-2X,[109] OLYP,[110] TPPSh[111] and MP2[112] methods) B3LYP, B3LYP-D and wB97XD were advocated to predict the correctly the spin ground state of the reactant and intermediates compared to experimental data available for the complex **2**.[94] Here we restrict our calculations only to two functionals, one is a plain B3LYP and the other is B3LYP-D functional (also called B3LYP-D2) incorporating dispersion correction of Grimme *et al.*[105–107] All the geometry optimizations are performed using the B3LYP and the B3LYP-D functionals.[105–107] Both the functionals have proven track-record of predicting the structures and the energetics accurately for such metal mediated catalytic reactions[94,113–126] and between the two the dispersion corrected functional is found to be superior[126] for spin state energetics. The dispersion corrected functionals tend to favour low-spin complexes over high-spin as the electron density of low-spin complexes are compact, which gives raise to larger r^{-6} attraction between metal and the ligand.

The LACVP basis set comprising LanL2DZ – Los Alamos effective core potential for Fe[127–130] and a 6-31G basis set for the other atoms (hydrogen carbon, nitrogen and oxygen)[131] (B-I) has been employed for the geometry optimization. Single point energy calculations were performed on the optimized geometries using a TZVP basis set (B-II) on all atoms.[132,133] The solvation energies have been incorporated using a PCM solvation model employing acetonitrile as the solvent. Frequency calculations at the B-I level were performed to verify that the optimized structures are minima on the potential-energy surface (PES) and also to obtain free energy corrections to the electronic energy computed at the TZVP level. Thus all the reported DFT energies are B3LYP-D (B3LYP in ESI†) solvation energies at B-II level incorporating free energies correction at the B-I level computed at room temperature (298.15 K). The transition states were verified by animating the single negative frequency corresponding to the reaction coordinate by using visualization software such as Molden.[134,135] The fragment approach available in Gaussian 09 is employed in case of radical intermediates. $^{mult}\mathbf{A}_{isomer}$ indicates a notation where **A**, mult and isomer stand for species name, total multiplicity and isomer (*cis* or *trans*).

3 Results and discussion

On the basis of the experimental studies[21,22,95] and earlier theoretical reports,[94] a schematic mechanism for the generation of Fe^{V}=O or Fe^{IV}=O species from the Fe^{III}–OOH species is depicted in Scheme 2. The Fe^{III}–OOH species itself is an unlikely oxidant in this chemistry as experiments suggest that this species degrades after which the hydroxylation reaction initiates.[21,22,94] Our earlier study on **2** also suggests that the barrier heights involved with the Fe^{III}–OOH species are too high to realistically perform the hydroxylation reaction with the benzoic acid.[94] This seems to suggest that the Fe^{III}–OOH undergoes homo or heterolytic cleavage of the O···O bond generating transient Fe^{IV}=O or Fe^{V}=O species. Thus these two species are potential oxidants in this chemistry.

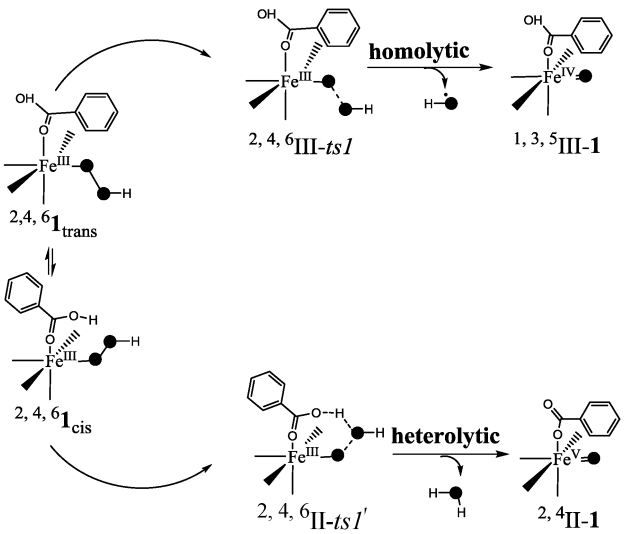

Scheme 2 The schematic mechanism for the formation of high-valent intermediates starting from Fe^{III}–hydroperoxo species.

Formation of the $[(BPMEN)(PhCOO)Fe^{V}{=}O]^{2+}$ and $[(BPMEN)(PhCOOH)Fe^{IV}{=}O]^{2+}$ oxidants

The $[Fe^{III}–OOH]^{2+}$ complex is the starting oxidant which is fully characterized by experiment as a low-spin S = 1/2 ferric species.[21,136,137] There are two possible isomers (*cis* and *trans*) based on the orientation of the –OH group of benzoic acid and the –OOH group. In the *cis* isomer, both the –OH group of benzoic acid and the –OOH group are on the same side and interact *via* H-bonding interaction while they are turned away in opposite direction to avoid this weak interaction in case of the *trans*-isomer (see Fig. 1 and Scheme 2). The computed energetics using B3LYP and B3LYP-D for different spin states for the Fe^{III}–OOH, Fe^{IV}=O and Fe^{V}=O are shown in Fig. 2. For the Fe^{III}–OOH, B3LYP-D predicts a low spin $^{2}\mathbf{1}_{cis}$ ground state with the $^{6}\mathbf{1}_{cis}$ being at 1.8 kJ mol^{-1} while B3LYP predicts a high-spin $^{6}\mathbf{1}_{cis}$ ground state with the $^{2}\mathbf{1}_{cis}$ being at 12.8 kJ mol^{-1} higher in energy. Here B3LYP-D yields the correct ground state consistent with the EPR measurements carried out on $[(BPMEN)Fe^{III}–OOH(CH_3CN)]^{2+}$ species.[21,137] This illustrates the need of dispersion in predicting the correct spin ground state of such species.

For the *trans*-isomer on the other hand both B3LYP and B3LYP-D predict a $^{6}\mathbf{1}_{trans}$ ground state (see Fig. 2). However this

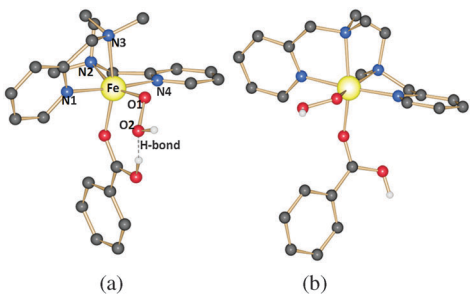

Fig. 1 B3LYP-D optimized structure of (a) $^{6}\mathbf{1}_{cis}$ and (b) $^{6}\mathbf{1}_{trans}$ species.

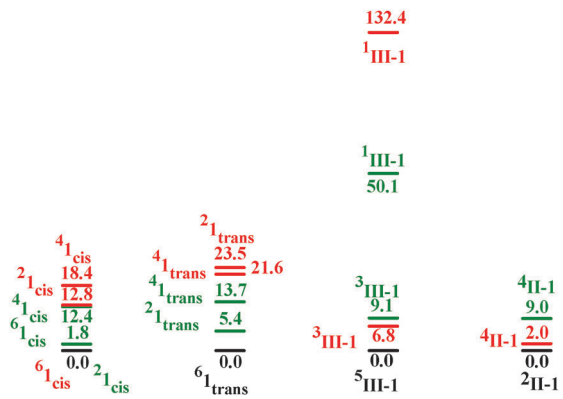

Fig. 2 B3LYP-D (olive) and B3LYP (red) computed spin state energies for *cis*-Fe^{III}–OOH, *trans*-Fe^{III}–OOH, Fe^{IV}=O and Fe^{V}=O species.

isomer is 23.4 kJ mol^{-1} higher in energy compared to the *cis*-isomer. The optimized structural parameters and spin state energetic computed are consistent with earlier reports.[94] A strong H-bonding interaction is formed between the –COOH group of benzoic acid and distal oxygen of the peroxo group and this interaction stabilizes the *cis*-isomer over the *trans*-isomer and also switches the ground state from S = 1/2 to 5/2 as we go from *cis* to *trans*. This subtle spin switching within the isomer is due to the fact that the computed energetics lie within the range expected for spin-crossover compounds[138] and thus minor perturbations are strong enough for spin state alterations.[139]

O···O bond heterolysis

Here we have attempted both homolysis and heterolysis of the O···O bond of the Fe^{III}–OOH species and the starting point for these are the corresponding *trans* and *cis*-isomers respectively. In heterolysis, acid-assisted cleavage generates water molecules leading to the formation of transient Fe^{V}=O species. The optimized structure of the transition state corresponding to this reaction at the doublet surface is shown in Fig. 3a (see also Fig. S1a of the ESI†). The computed potential energy surface for this reaction is shown in Fig. 4 (see also Fig. S2 of the ESI†). The barrier heights computed are 73.6, 103.9 and 113.1 kJ mol^{-1} for the doublet (^{2}II-ts1), sextet (^{6}II-ts1) and quartet (^{4}II-ts1) spin surfaces and the doublet is computed to have the lowest energy barrier among all the computed spin surfaces. Interestingly, as the ground state is predicted to be a sextet ($^{6}\mathbf{1}_{cis}$) by B3LYP, the reaction requires a minimum energy crossing point (MECP)[140] between the doublet and the sextet surface in B3LYP (see Fig. S2 of the ESI†) while no such requirements are present when the dispersion effects are incorporated. The computed energy barrier between these two functionals suggests that dispersion has significant impact on the energy barrier as the lowest energy transition state is *ca.* 10 kJ mol^{-1} lower in energy upon addition of dispersion.

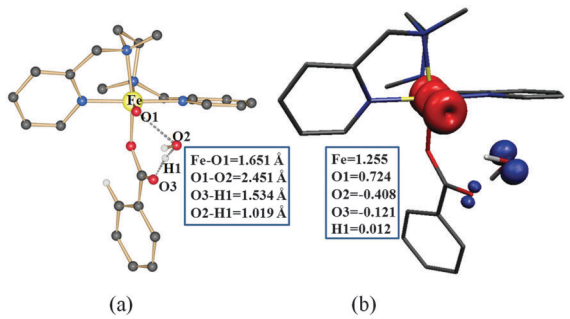

Fig. 3 B3LYP-D computed (a) optimized structure and (b) spin density plot for the ^{2}II-ts1 species.

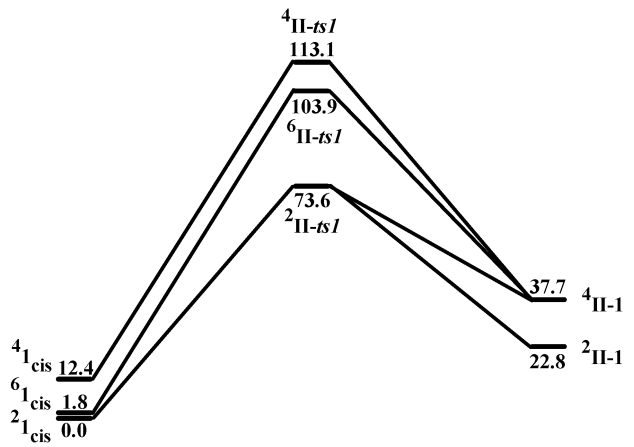

Fig. 4 B3LYP-D computed potential energy surface (ΔG in kJ mol^{-1}) for the O···O bond cleavage starting from $\mathbf{1}_{cis}$ species.

In the ^{2}II-ts1 the O···O bond elongates to 2.451 Å and Fe–O bond shortens to 1.651 Å compared to 1.519 Å and 1.825 Å of the reactant. All the computed bond parameters are shown in Table S1 of the ESI.† The O(1)···O(2) bond is almost broken in the doublet surface (^{2}II-ts1) and the water molecule is formed by accepting the proton from the benzoic acid. However the O(1)···O(2) bonds in the quartet and the sextet states are still intact. Thus the ^{2}II-ts1 is product-like however transitions states on other surfaces are reactant-like transition states. Both the functionals predict a similar trend here with some alteration in the structural parameters. The spin density plot of transition state (^{2}II-ts1) is shown in Fig. 3b (see also Fig. S1b of the ESI,† see Table S2, ESI,† for $\langle S^{**}2\rangle$ values and the corresponding spin contamination detected at the transition state) and this clearly indicates that the O···O bond cleaves heterolytically, as a significant difference in spin population is noted between O(1) and O(2) atoms. Since O(1) and O(2) have opposite spin densities, this suggests spin polarization is dominant in the transition state leading to O···O bond heterolysis. Although both the functionals yield a similar picture here, the absolute variations in the magnitudes of spin densities are larger in the B3LYP-D compared to B3LYP, suggesting in fact that dispersion drives the transition state much closer to the product. The heterolysis is also supported by the computed charges on the oxygen atoms (see Table S3 of the ESI†).

After the O···O bond cleaves heterolytically, this generates the Fe^{V}=O (^{2,4}II-**1**) species and its formation is found to be endothermic in nature (28.6 kJ mol^{-1}; see Fig. 4). The Fe^{V}=O has a doublet ground state with the quartet ground state higher in energy (see Fig. 4). The computed ground state-excited state energy gap and structures are consistent with previous theoretical and experimental reports.[91,94,96–100] The lying 14.9 kJ mol^{-1} with S = 1/2 being the computed Fe–O bond lengths also agree with the reported X-ray structure of the Fe^{V}=O species with different ligand architectures (see Table S1 of ESI,† where comparisons to available experimental structures are made).[91]

O···O bond homolysis

Similar to the Fe^{V}=O, here we are aiming to generate the Fe^{IV}=O oxidant and we have taken the $\mathbf{1}_{trans}$ as the reactant for the cleavage of O···O bond. The O···O bond cleavage transition state has been computed for all three spin states (see Fig. 5). The barrier height is computed to be 107.2, 114.2 and 237.5 kJ mol^{-1} for the sextet (^{6}II-ts1), doublet (^{2}II-ts1) and quartet (^{4}II-ts1) spin surfaces. In the ^{6}III-ts1 state, the Fe–O bond is relatively long (1.672 Å *vs.* 1.915 Å of the reactant) while the

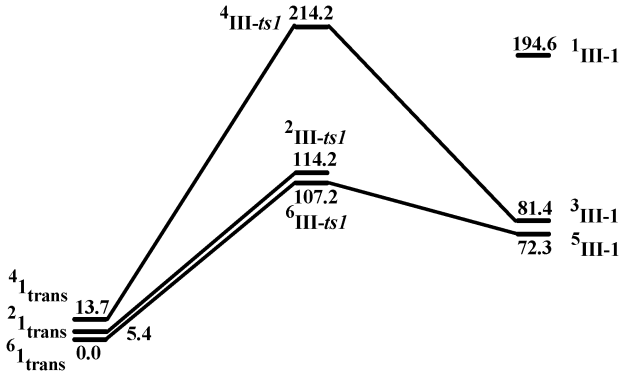

Fig. 5 B3LYP-D computed potential energy surface (ΔG in kJ mol^{-1}) for the O···O bond cleavage starting from $\mathbf{1}_{trans}$ species.

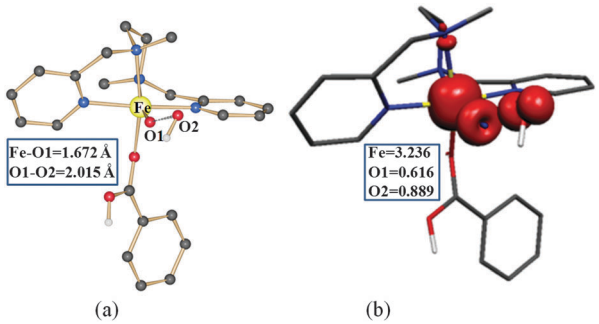

Fig. 6 B3LYP-D computed (a) optimized structure and (b) spin density plot of the ground state (^{6}III-ts1).

O···O bond is already cleaved (2.015 Å *vs.* 1.483 Å of the reactant) as shown in Fig. 6a (see also Fig. S3a in B3LYP, Fig. S4 and Table S1 of the ESI†). To understand whether the O···O bond cleavage is homolytic or heterolytic, the spin density of the ^{6}III-ts1 is plotted (see Fig. 6b and Fig. S3b of the ESI†). Here significant spin densities on both the proximal and distal oxygen atoms are noted (0.597 and 0.868); as both the O(1) and O(2) atoms have significant spin densities, this denotes development of radical character and suggest that the O···O bond cleaves in a homolytic fashion leading to a Fe^{IV}=O species. This is also supported by the computed charges on both the oxygen atoms (see Table S3 of the ESI†). Here the sextet is found to have the lowest energy barrier among all the spin surfaces and suggests that homolysis is preferentially carried out in a high-spin surface while heterolysis preferred in the doublet surface.

The orbital analysis for the homolysis *vs.* heterolysis of O···O bond from ^{6}**1**, ^{4}**1** and ^{2}**1** species are shown in Scheme 3. This is developed by analysing the frontier orbitals of the species involved (see Fig. S5–S8 of ESI,† for Eigen-value plot of the corresponding species).

This orbital analysis readily explains why homolysis is preferentially carried out in the sextet (^{6}**1**) state while heterolysis is occurring at the doublet surface. At doublet (^{2}**1**) surface, heterolysis generates ^{2}II-**1** of the Fe^{V}=O species without any demand for spin reversal, however homolysis at the same surface generates ^{1}III-**1** of the Fe^{IV}=O species which is very high in energy. On the other hand at the ^{6}**1** surface homolysis generates ^{5}III-**1** of the Fe^{IV}=O species which is found to be the ground state here. Heterolysis on ^{6}**1** surface generates ^{4}II-**1** of the Fe^{V}=O species which is the excited state and requires also a spin-reversal. The ^{4}**1** of the Fe^{III}–OOH generates ^{2}II-**1** of the Fe^{V}=O with a spin reversal or a ^{3}III-**1** of Fe^{IV}=O without any demand for spin reversal, but these transition states are the highest lying in the computed potential energy surface. A homolytic cleavage of the O···O bond results in the formation of the Fe^{IV}=O species (^{5,3,1}III-**1**). For the Fe^{IV}=O (III-**1**) species, a quintet state is found to be the ground state with the triplet and the singlet being at 9.1 and 50.1 kJ mol^{-1} higher in energy (see Fig. 5). Although the triplet state has been estimated as the ground state for the $[Fe^{IV}(O)(BPMEN)(NCCH_3)]^{2+}$ species,[18,141–144] for the $[Fe^{IV}(O)(BPMEN)(PhCOOH)]^{2+}$ species (III-**1**), experimental data is unavailable. Our calculations suggest that the triplet is indeed the ground state for the $[Fe^{IV}(O)(BPMEN)(NCCH_3)]^{2+}$ species with the quintet state being at 13.5 kJ mol^{-1} higher in energy and this is in accordance with the experimental observations.[145] The quintet (^{5}III-**1**) states of the Fe^{IV}=O complexes are however characterized with different ligand architectures.[146–151] The formation of the Fe^{IV}=O species is also found to be endothermic by 72.3 kJ mol^{-1} (69.1 in B3LYP).

Considering the fact that both the Fe^{IV}=O and Fe^{V}=O have been proposed as the possible oxidant in the hydroxylation reaction, we have proposed a different route to generate the oxidant exclusively. For example, the Fe^{IV}=O oxidant is generated *via* O···O homolysis of the *trans*-Fe^{III}–OOH while the Fe^{V}=O oxidant is generated *via* O···O heterolysis of the *cis*-isomer. Since the *cis*-isomer is stabilized by 23.4 kJ mol^{-1} over the *trans*-isomer and the conversion of *cis* to *trans* requires 51.9 kJ mol^{-1} (see Fig. S12 of the ESI†), this conversion is unlikely.

Between homolysis *vs.* heterolysis, the heterolysis is favoured by 33.6 kJ mol^{-1} (not accounting the energy penalty for producing the *trans*-isomer from the *cis*-isomer). The formation of the Fe^{V}=O is also thermodynamically more favourable over the corresponding Fe^{IV}=O species by a margin of 49.5 kJ mol^{-1}. All the above facts synchronize with the experimental observation and unequivocally suggest that the Fe^{V}=O is the potential oxidant in this chemistry which triggers this catalytic transformation.[94]

Mechanism of *ortho*-hydroxylation

A small inverse kinetic isotopic effect observed for the *ortho*-hydroxylation for complex **1** suggests that electrophilic attack accompanied by sp^2/sp^3 rehybridization is taking place during the course of the reaction and the C–H activation step can be ruled out.[21,94] Our earlier theoretical study on complex 2 also suggests that electrophilic attack is energetically preferred over the C–H activation step.[94] Bearing in mind these reports, a schematic mechanism for the *ortho*-hydroxylation has been adapted (see Scheme 4).

First the ferryl oxygen attacks the *ortho*-position of the benzoic acid *via* the transition state (II-ts2). This step requires just 2.7 kJ mol^{-1} in the doublet surface while in the quartet the barrier height is estimated to be 13.5 kJ mol^{-1} (see Fig. 7). The

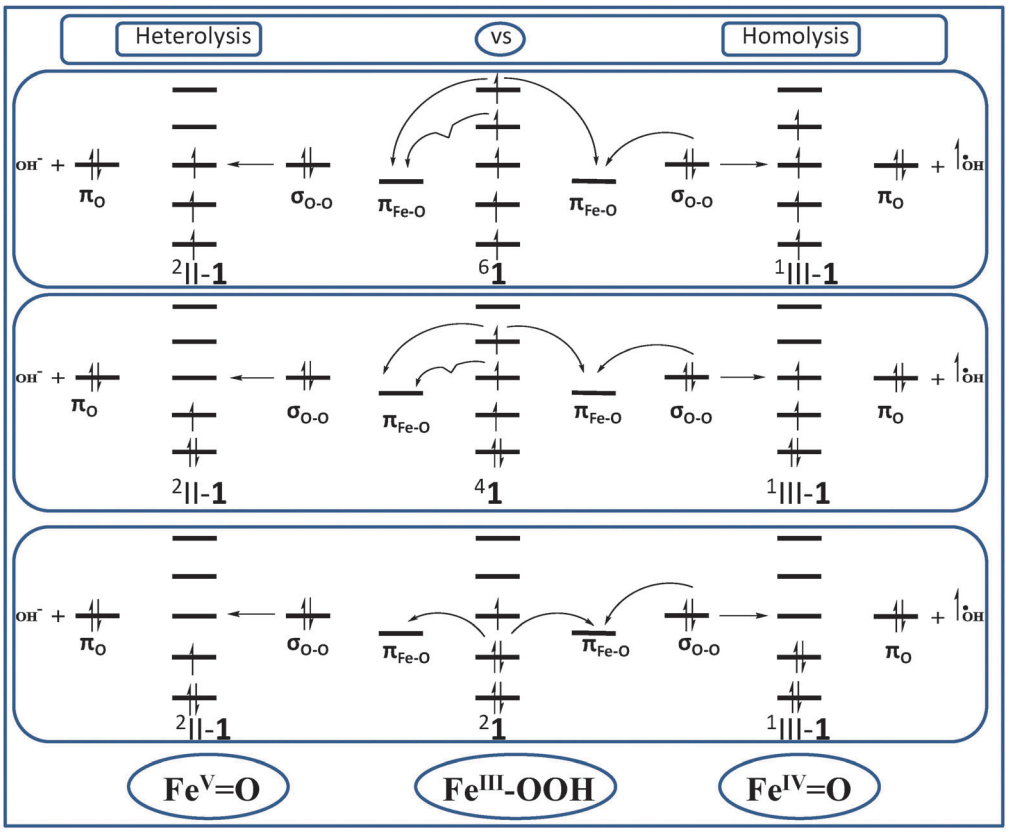

Scheme 3 Analysis of orbitals during homolysis and heterolysis of the Fe^{III}–OOH species.

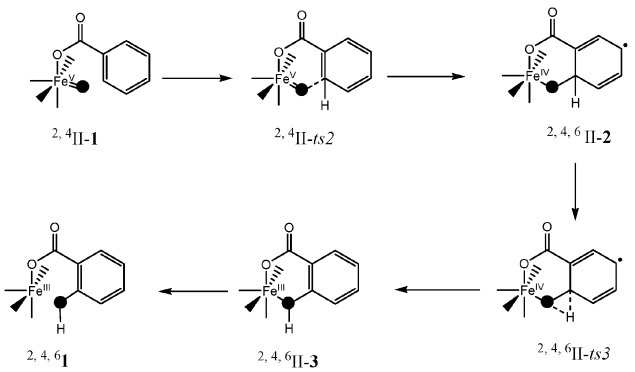

Scheme 4 Adapted schematic mechanism for *ortho*-hydroxylation by the Fe^{V}=O species.

Fe–O bond slightly elongates from 1.654 to 1.656 Å, forming a new partial O···C bond in the transition state (^{2}II-ts2) (see Fig. 8a). The newly forming O···C_{ph} bond is 2.680 Å; both these parameters suggest that this is an early transition state and resembles the reactant species. The computed spin density plot of $^{2}II_{b}$-ts2 indicates a radical character on the *ortho*-carbon (ρ = −0.179; see Fig. 8b) has been developed at this transition state suggesting in fact that II-2 species is a radical species.

There are five possible spin states for intermediate II-2 due to the coupling of unpaired electrons of iron with the radical centre. Among the computed states, the ^{6}II-**2** (see Fig. S11a of the ESI†) is computed to be the ground state and the formation of this intermediate is exothermic by 122.6 kJ mol^{-1}.[152] The other two states, ^{4}II-**2** and the ^{2}II-**2** states are 114.8 and 94.8 kJ mol^{-1} higher in energy respectively (see Fig. 7 and Fig. S13 of the ESI†).

In the next step, *via* II-ts3 from the II-2 species, hydrogen migration takes place to restore the aromaticity of the benzene ring which was lost upon the electrophilic attack. This is essentially a sp^2 (reactant) to sp^3 (II-2) and then to sp^2 (II-3) rehybridization and supports the small inverse KIE values observed.[21] Here again our result shows that the sextet state (^{6}II-ts3) is computed to be ground state (Fig. 8c) and the computed barrier height here is 35.9 kJ mol^{-1}. Since the intermediate formation is highly exothermic, this transition state is essentially barrier-less from the reactant species. In this transition state (^{6}II-ts3), the C–H bond is elongating and the O–H bond is forming. In the next step the hydrogen migration completes leading to the formation of the *ortho*-hydroxylated intermediate II-3. For the species II-3 as well, the sextet (see Fig. S14b of the ESI†) is computed to be the ground state and this step is excessively exothermic by 269.9 kJ mol^{-1}. In the next step, the Fe–O bond breaks leading to the desired *ortho*-hydroxylated product (^{2,4,6}**1**). This step is also exothermic from the earlier intermediate suggesting in fact that once the electrophilic attack takes place, the reaction proceeds faster leading to the generation of the *ortho*-hydroxylated product.

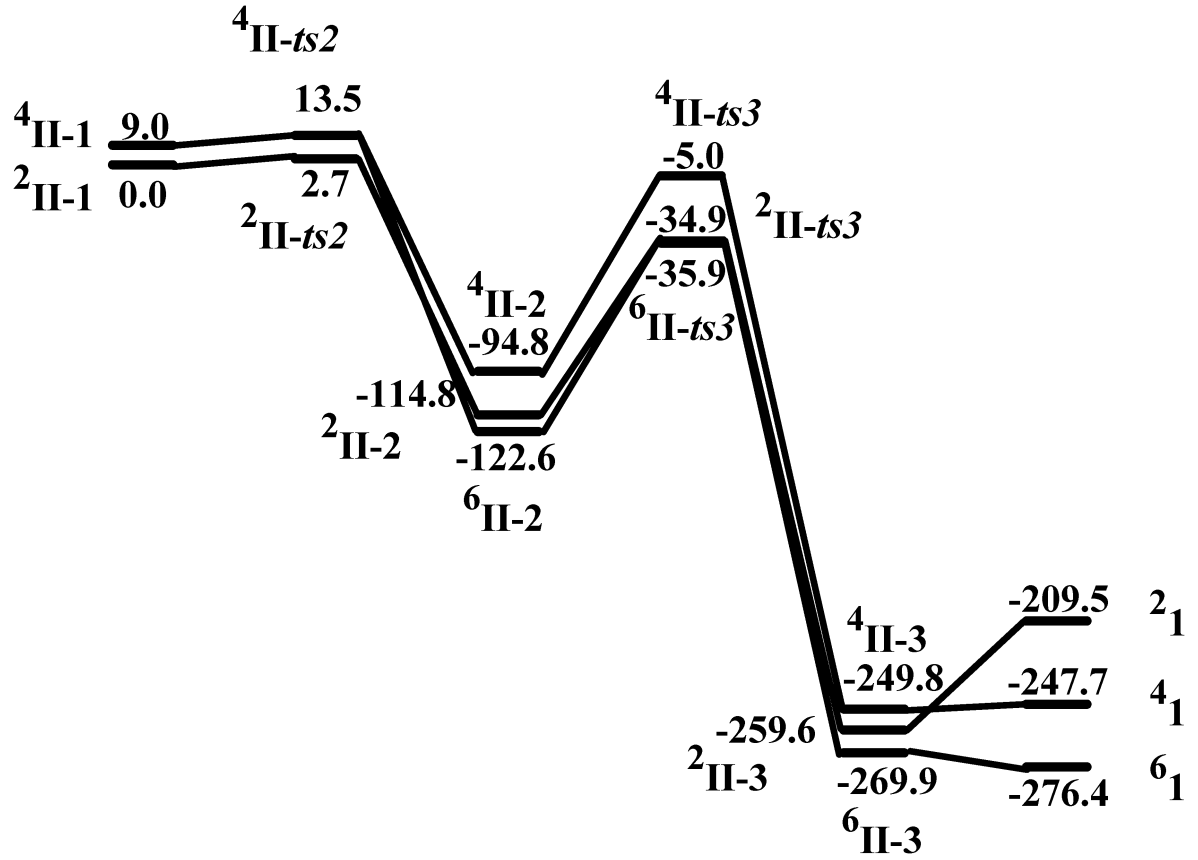

Fig. 7 B3LYP-D computed potential energy surface (ΔG in kJ mol^{-1}) for the electrophilic attack pathway for the *ortho*-hydroxylation reaction.

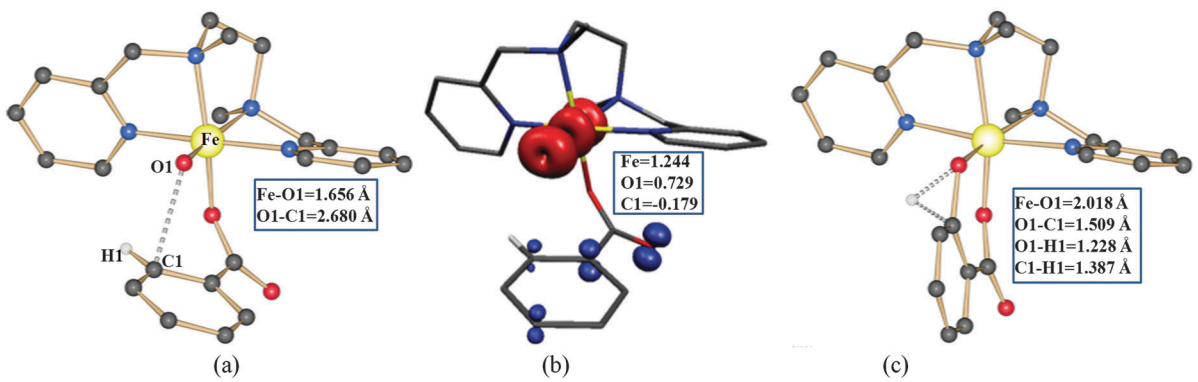

Fig. 8 B3LYP-D optimized structure of the ground state of (a) ^{2}II-ts2, (b) spin density plot of ^{2}II-ts2 and (c) optimized structure of ^{6}II-ts3.

Importance of the ligand design: electronic structure differences driven by ligand design between II-1 and II-1(2) species

For the TPA ligand system, there are two positional isomers for the $[(TPA)(C_6H_5COO)Fe^{V}{=}O]^{2+}$ (II-**1**(**2**)) species where the –OOH group *trans* to tertiary amine is found to be the lowest in energy by 8.8 kJ mol^{-1}.[21] For this species as well S = 1/2 (^{2}II-**1**(**2**)) is predicted to be the ground state with the S = 3/2 lying at 12.1 kJ mol^{-1} (0.6 using B3LYP; Fig. S6, ESI†). The same gap with the BPMEN ligand (II-**1**) system is 9.0 kJ mol^{-1} (2.0 in B3LYP) revealing that the reactivity differences are unlikely be due to the ground state–excited state gap but due to the intrinsic electronic differences between these two species.

Although both II-**1** and II-**1**(**2**) species are structurally alike, there are some structural differences that attribute differential electrophilicity of the ferryl oxygen atom in these species. Particularly the II-**1** species contains one pyridine ring that is perpendicular to the Fe=O bond while the other pyridine aligns parallel to the Fe=O bond.[20] In the II-**1**(**2**) species however two of the pyridine rings are parallel to the Fe=O bond while one pyridine is perpendicular to the Fe=O bond

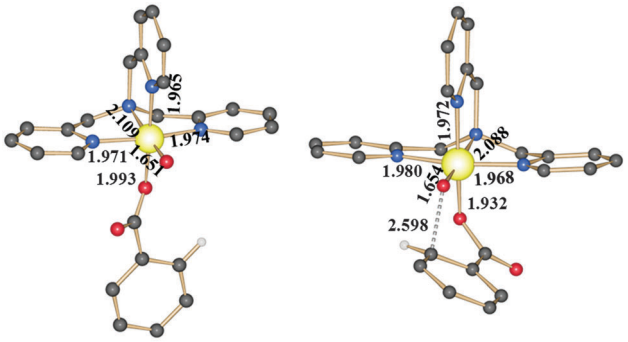

Fig. 9 B3LYP-D computed optimized of ^{2}II-**1**(**2**) and ^{2}II$_{b}$-ts2(**2**) species.[94]

(see Fig. 9a and Fig. S8 of the ESI†). The differences in reactivity between these two ligand systems are likely to arise due to these structural differences as other structural aspects are very similar to one another.

Apart from the regular structure described for II-**1** species ([(BPMEN)(C_6H_5COO)Fe^{V}=O]$^{2+}$; isomer A or II-**1A** (see Fig. 10)), to probe the role of pyridine ring orientation, we have generated two more isomers for this species where both the pyridine rings align either parallel (isomer B; II-**1B**) or perpendicular (isomer C; II-**1C**) to the Fe=O bond (see Fig. 11 and Fig. S10 of the ESI†). Interestingly for both the isomers B and C, an S = 3/2 is found to be the ground state with the S = 1/2 state found to lie at 22.6 and 45.7 kJ mol^{-1} for B and C respectively. Both isomers

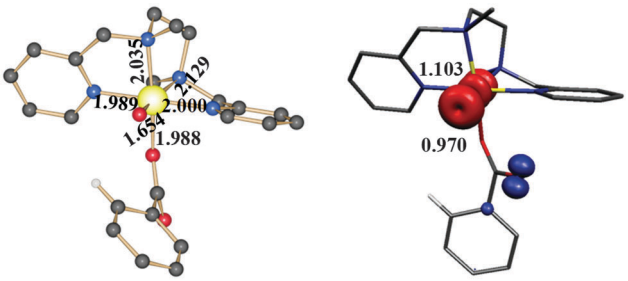

Fig. 10 B3LYP-D computed optimized and spin density plot of ground state of the ^{2}II-**1**.

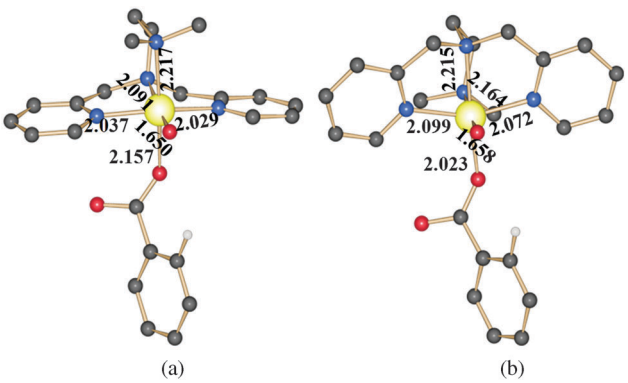

Fig. 11 B3LYP-D computed optimized structures of (a) ^{4}II-**1B** and (b) ^{4}II-**1C**.

B and C are found to be high-lying compared to A by an energy margin of 35.9 and 43.6 kJ mol^{-1} respectively. These energetics clearly illustrate that the orientation of the pyridine rings play an important role in the stability of these species.

The Fe–N(py) distances also drastically vary based on the orientation in all four structures (II-**1A**, II-**1B**, II-**1C** and II-**1**(**2**)) with longer Fe–N distances found when the pyridine rings are parallel to the Fe=O bond. This is due to the fact that the pyridine π-orbitals strongly mixes with the $(\pi_{Fe(dyz)-O(py)})^*$ orbital when it is aligned parallel to the Fe=O bond. The perpendicular orientation prevents the π-orbitals of pyridine to mix with the $(\pi_{Fe(dyz)-O(py)})^*$ orbital (see Fig. S11 of the ESI†).

This mixing with π(Fe–O)* frontier MO stabilizes the Fe^{V}=O species and provide a more delocalized description for the unpaired electron (see Fig. 12). An eigen-value plot incorporating the energies of d-based orbitals for species II-**1** and II-**1**(**2**) is shown in Fig. 12. For both the species the $(\delta_{xy})^2(\pi_{Fe(dyz)-O(py)})^{*1}$ configuration is detected for the ground state. The $(\pi_{Fe(dyz)-O(py)})^*$ orbital in II-**1** is more destabilized than that in species II-**1**(**2**). This is again associated with the fact that II-**2** has two parallel pyridines stabilizing the $(\pi_{Fe(dyz)-O(py)})^*$orbital compared to II-**1** which possess only one parallel pyridine ring.

The α-hydrogen atom of the pyridine ring is also in a H-bonding interaction with the ferryl oxo species when the pyridine rings are parallel to the Fe=O bond. This is also reflected in the spin densities of the ferryl oxygen atoms where the magnitude of the spin density is found to correlate to the number of pyridine rings being either parallel or perpendicular to the Fe=O bond (see Table S4 of the ESI†). This analysis suggests that the electrophilicity of the ferryl oxygen atoms decreases in the following order: II-**1C** > II-**1A** > II-**1**(**2**) > II-**1B**. This trend rationalizes the observed difference in reactivity between species **1** and **2** and suggests that (i) the ligand possessing pyridine parallel to the Fe=O bond can help to stabilize the transient species or can help to enhance the $t_{1/2}$ times so that these species can be trapped and a thorough spectroscopic and other characterization can be performed (ii) the ligand possessing pyridine perpendicular to the Fe=O leads to a localized Fe=O bond character and there are likely to be stronger oxidants. In the next section we test the reactivity of these two species towards *ortho*-hydroxylation to probe further the observed reactivity pattern.

Importance of ligand design: reactivity towards the *ortho*-hydroxylation of benzoic acid

The computed PES for the *ortho*-hydroxylation of benzoic acid by complexes **1** and **2** is given in Fig. 13 (see also Fig. S15 of the ESI†). Starting from the *cis*-isomer of each, the heterolytic cleavage of the O···O bond is predicted to have a barrier height of 69.9 kJ mol^{-1} for the complex **2** while complex **1** has a barrier height of 73.6 kJ mol^{-1}. A lower barrier for complex **2** suggests that formation of Fe^{V}=O species is faster with the TPA ligand system than with the BPMEN ligand system. The electrophilic attack on the benzene ring by the Fe^{V}=O species is found to be the rate limiting step for both species and this has a barrier

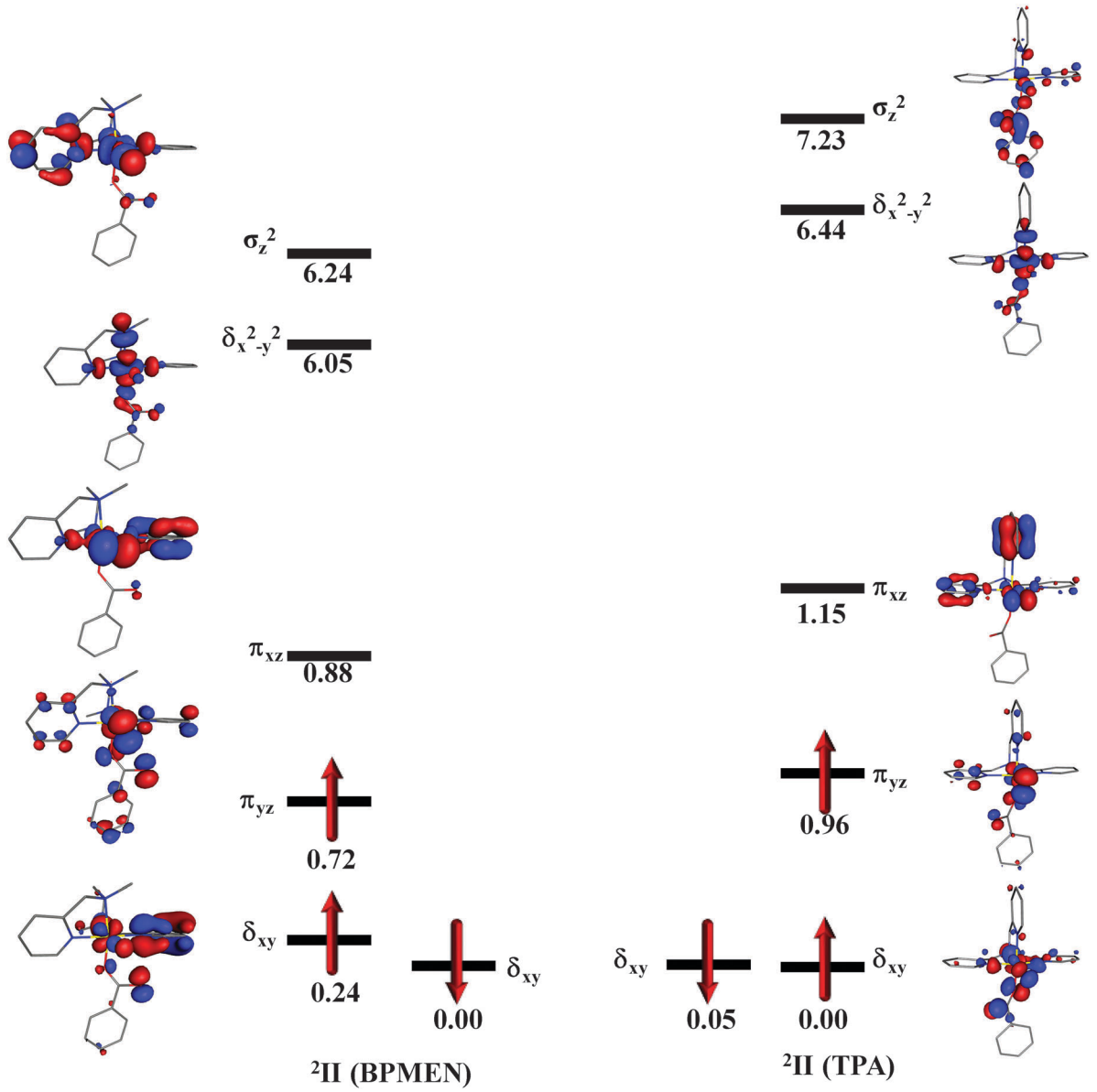

Fig. 12 B3LYP-D computed Eigen-value plot incorporating energies computed for d-based orbitals for II-**1** and II-**1**(**2**) species at doublet surface (energies are given in eV).

height of just 2.7 kJ mol^{-1} for BPMEN (II-1) while the it is 5.3 kJ mol^{-1} for the TPA system (II-**1**(**2**); see Fig. 9b for ^2II_b-ts2(**2**)).

The TPA–Fe^{V}═O species always forms less exothermic intermediates and have slightly larger kinetic barrier for the rest of the reaction as shown in Fig. 13. This agrees with the experimental observation where complex **1** is found to be more reactive than complex **2**. Coincidently, the ratio of the product formation, 1.84, between these two systems (94% for 1 and 51% for **2**)[22] also matches with the ratio of the barrier heights computed for the rate determining step of the hydroxylation reaction (1.96).

Correlation to experiments

All our results are in agreement with the experiments where the Fe^{V}═O has been proposed as a potential oxidant for the *ortho*-hydroxylation of benzoic acid for both complexes **1** and **2**. Control experiments, particularly the reaction with the organic peroxide MPPH (2-methyl-1-phenyl-2-propyl hydroperoxide), suggests that the O···O bond of the Fe^{III}–OOH cleaves in a heterolytic fashion[21] and calculations suggest that in the tetradentate ligand system when the benzoic acid coordinates to the *cis*-position of the –OOH group, this leads to acid-assisted cleavage of the O···O bond leading to the formation of Fe^{V}═O species.

This has a much lower barrier than homolytic cleavage. Thus our calculations reiterate the fact that Fe^{V}═O is the likely oxidant in this chemistry. Our mechanistic studies reveal that ferryl oxygen attacks the benzene ring *via* electrophilic attack and this is also consistent with the small inverse kinetic isotopic effect values (k_H/k_D = 0.8)[21] determined by experiments.

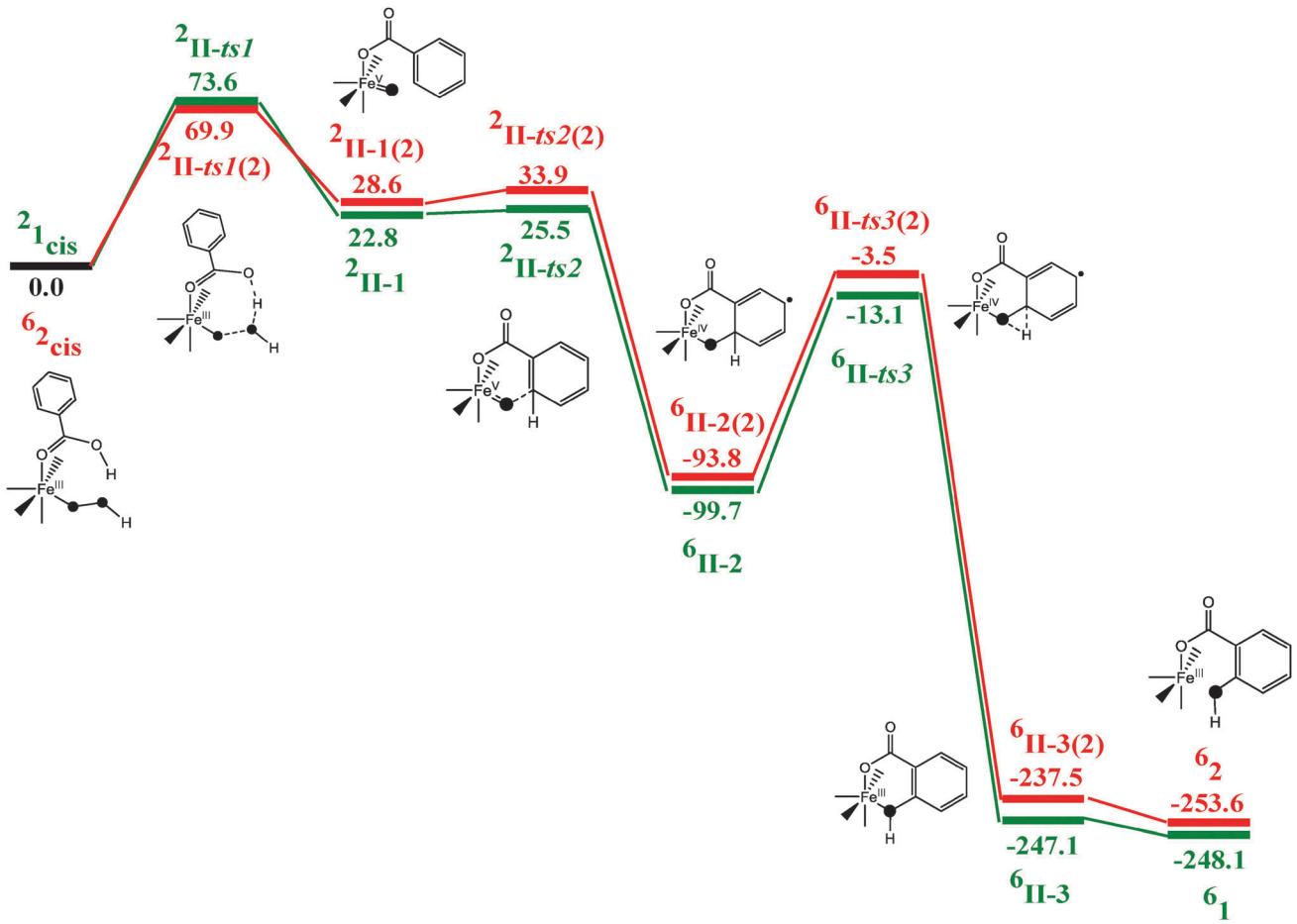

Fig. 13 B3LYP-D computed potential energy surface (ΔG in kJ mol^{-1}) (green for BPMEN and red for TPA[94]). All energies are in kJ mol^{-1}.

4 Conclusions

DFT calculations have been performed to explore the mechanism of the *ortho*-hydroxylation reaction of benzoic acid with $[(BPMEN)Fe^{III}–OOH]^{2+}$ species and compared its reactivity with $[(TPA)Fe^{III}–OOH]^{2+}$ species. Significant insights into the mechanistic aspect of these two systems are gained in this work. Particularly our work highlights the importance of ligand design to achieve greater reactivity for these species. Some salient conclusions derived from this work is summarized below.

(1) The dispersion corrected B3LYP functional is found to perform better in predicting the correct spin states for these high-valent iron-oxo species compared to B3LYP. B3LYP-D also yields lower energy barrier heights for the transition states compared to B3LYP and this implies that accurate estimation of the kinetics requires the incorporation of dispersion effects.

(2) The O···O bond heterolysis of Fe^{III}–OOH species is found to be an energetically favourable process for both the ligand systems studied. This suggest that the acidic protons present in the *cis*-position of the –OOH group leads to the generation of Fe^{V}=O species preferentially over the popular Fe^{IV}=O species.

The Fe^{V}=O species formed with both ligand systems preferentially undergoes electrophilic attack of the benzene ring leading to a transient radical intermediate. This suggests that the reaction proceeds *via* a radical pathway. The migration of a hydrogen atom from this intermediate leads to the formation of the *ortho*-hydroxylated product and these findings are consistent with the small KIE observed. The first electrophilic attack of the ferryl oxygen on the aromatic ring is found to be the rate determining step for both the species.

(3) The difference in reactivity between these two ligand systems studied are found to correlate with the orientation of the pyridine rings, with the pyridine ring parallel to the Fe=O bond found to interact with the $(\pi_{Fe(dyz)–O(py)})^{*}$ SOMO orbital leading to more delocalized densities and a less electrophilic ferryl oxygen character. This adds up to less reactivity. Our calculations predict that if both the pyridine rings of the BPMEN ligand systems are perpendicular, an enhanced reactivity may be achieved. Such modified ligand systems are known in the literature but *ortho*-hydroxylation of such systems has not been studied.[145,153,154]

To this end our calculations shows the reactivity of the non-heme iron system can be fine-tuned at will with designed ligand architectures. This underlines the importance of ligand design in this chemistry with two diverse goals, one to achieve a relatively stable reactive intermediates (such as Fe^{IV}=O or Fe^{V}=O species) in order to trap and thoroughly characterize them, and the other to achieve a transient but aggressive

oxidant which can perform the catalytic transformations with enhanced selectivity, efficiency and robustness.

Acknowledgements

GR would like to acknowledge the financial support from the Government of India through Department of Science and Technology (SR/S1/IC-41/2010; SR/NM/NS-1119/2011) and generous computational resources from Indian Institute of Technology-Bombay. AA thanks CSIR for a SRF fellowship.

Notes and references

1 R. A. Sheldon and J. K. Kochi, *Metal-Catalyzed Oxidations of Organic Compounds*, Academic Press, New York, 1981.
2 T. Punniyamurthy, S. Velusamy and J. Iqbal, *Chem. Rev.*, 2005, **105**, 2329–2364.
3 A. Fishman, Y. Tao, L. Rui and T. K. Wood, *J. Biol. Chem.*, 2005, **280**, 506–514.
4 M. H. Sazinsky, J. Bard, A. Di Donato and S. J. Lippard, *J. Biol. Chem.*, 2004, **279**, 30600–30610.
5 K. H. Mitchell, C. E. Rogge, T. Gierahn and B. G. Fox, *Proc. Natl. Acad. Sci. U. S. A.*, 2003, **100**, 3784–3789.
6 L. J. Murray and S. J. Lippard, *Acc. Chem. Res.*, 2007, **40**, 466–474.
7 T. Flatmark and R. C. Stevens, *Chem. Rev.*, 1999, **99**, 2137–2160.
8 P. F. Fitzpatrick, *Biochemistry*, 2003, **42**, 14083–14091.
9 M. M. Abu-Omar, A. Loaiza and N. Hontzeas, *Chem. Rev.*, 2005, **105**, 2227–2252.
10 P. C. A. Bruijnincx, G. van Koten and R. J. M. K. Gebbink, *Chem. Soc. Rev.*, 2008, **37**, 2716–2744.
11 L. Ridder, J. N. Harvey, I. M. C. M. Rietjens, J. Vervoort and A. J. Mulholland, *J. Phys. Chem. B*, 2003, **107**, 2118–2126.
12 M. J. Kang, W. J. Song, A. R. Han, Y. S. Choi, H. G. Jang and W. Nam, *J. Org. Chem.*, 2007, **72**, 6301–6304.
13 S. P. de Visser, D. Kumar, S. Cohen, R. Shacham and S. Shaik, *J. Am. Chem. Soc.*, 2004, **126**, 8362–8363.
14 D. Kumar, S. P. de Visser and S. Shaik, *J. Am. Chem. Soc.*, 2003, **125**, 13024–13025.
15 C. Walling and R. A. Johnson, *J. Am. Chem. Soc.*, 1975, **97**, 363–367.
16 D. T. Sawyer, A. Sobkowiak and T. Matsushita, *Acc. Chem. Res.*, 1996, **29**, 409–416.
17 S. P. de Visser, K. Oh, A.-R. Han and W. Nam, *Inorg. Chem.*, 2007, **46**, 4632–4641.
18 J. U. Rohde, J. H. In, M. H. Lim, W. W. Brennessel, M. R. Bukowski, A. Stubna, E. Munck, W. Nam and L. Que Jr., *Science*, 2003, **299**, 1037–1039.
19 J. England, Y. Guo, E. R. Farquhar, V. G. Young Jr., E. Munck and L. Que Jr., *J. Am. Chem. Soc.*, 2010, **132**, 8635–8644.
20 E. J. Klinker, J. Kaizer, W. W. Brennessel, N. L. Woodrum, C. J. Cramer and L. Que Jr., *Angew. Chem., Int. Ed.*, 2005, **44**, 3690–3694.
21 O. V. Makhlynets and E. V. Rybak-Akimova, *Chem. – Eur. J.*, 2010, **16**, 13995–14006.
22 O. V. Makhlynets, P. Das, S. Taktak, M. Flook, R. Mas-Balleste, E. V. Rybak-Akimova and L. Que Jr., *Chem. – Eur. J.*, 2009, **15**, 13171–13180.
23 B. E. Eser, E. W. Barr, P. A. Frantorn, L. Saleh, J. M. Bollinger, C. Krebs and P. F. Fitzpatrick, *J. Am. Chem.Soc.*, 2007, **129**, 11334–11335.
24 C. Krebs, D. G. Fujimori, C. T. Walsh and J. M. Bollinger, *Acc. Chem. Res.*, 2007, **40**, 484–492.
25 J. M. Bollinger and C. Krebs, *J. Inorg. Biochem.*, 2006, **100**, 586–605.
26 N. Y. Oh, M. S. Seo, M. H. Lim, M. B. Consugar, M. J. Park, J. U. Rohde, J. H. Han, K. M. Kim, J. Kim, L. Que Jr. and W. Nam, *Chem. Commun.*, 2005, 5644–5646.
27 O. Y. Lyakin, K. P. Bryliakov and E. P. Talsi, *Inorg. Chem.*, 2011, **50**, 5526–5538.
28 C. M. Bathelt, L. Ridder, A. J. Mulholland and J. N. Harvey, *J. Am. Chem. Soc.*, 2003, **125**, 15004–15005.
29 H. Hirao, L. Que Jr., W. Nam and S. Shaik, *Chem. – Eur. J.*, 2008, **14**, 1740–1756.
30 C. V. Sastri, J. Lee, K. Oh, Y. J. Lee, J. Lee, T. A. Jackson, K. Ray, H. Hirao, W. Shin, J. A. Halfen, K. Kim, L. Que Jr., S. Shaik and W. Nam, *Proc. Natl. Acad. Sci. U. S. A.*, 2007, **104**, 19181–19186.
31 W. J. Song, Y. J. Sun, S. K. Choi and W. Nam, *Chem. – Eur. J.*, 2006, **12**, 130–137.
32 C. V. Sastri, M. S. Seo, M. J. Park, K. M. Kim and W. Nam, *Chem. Commun.*, 2005, 1405–1407.
33 S. P. de Visser, *J. Am. Chem. Soc.*, 2010, **132**, 1087–1097.
34 S. J. Kim, R. Latifi, H. Y. Kang, W. Nam and S. P. de Visser, *Chem. Commun.*, 2009, 1562–1564.
35 D. Kumar, L. Tahsini, S. P. de Visser, H. Y. Kang, S. J. Kim and W. Nam, *J. Phys. Chem. A*, 2009, **113**, 11713–11722.
36 D. Kumar, S. P. de Visser, P. K. Sharma, E. Derat and S. Shaik, *J. Biol. Inorg. Chem.*, 2005, **10**, 181–189.
37 S. Shaik, D. Kumar, S. P. de Visser, A. Altun and W. Thiel, *Chem. Rev.*, 2005, **105**, 2279–2328.
38 A. M. Liu, Y. Jin, J. Y. Zhang, B. J. Brazeau and J. D. Lipscomb, *Biochem. Biophys. Res. Commun.*, 2005, **338**, 254–261.
39 S. K. Lee, J. C. Nesheim and J. D. Lipscomb, *J. Biol. Chem.*, 1993, **268**, 21569–21577.
40 X. P. Shan and L. Que Jr., *J. Inorg. Biochem.*, 2006, **100**, 421–433.
41 S. Shaik, S. P. de Visser and D. Kumar, *J. Biol. Inorg. Chem.*, 2004, **9**, 661–668.
42 F. Ogliaro, S. P. de Visser, S. Cohen, P. K. Sharma and S. Shaik, *J. Am. Chem. Soc.*, 2002, **124**, 2806–2817.
43 P. K. Sharma, S. P. de Visser and S. Shaik, *J. Am. Chem. Soc.*, 2003, **125**, 8698–8699.
44 M. J. Park, J. Lee, Y. Suh, J. Kim and W. Nam, *J. Am. Chem. Soc.*, 2006, **128**, 2630–2634.
45 B. Meunier, *Chem. Rev.*, 1992, **92**, 1411–1456.
46 N. Kitajima, H. Fukui and Y. Moro-oka, *J. Chem. Soc., Chem. Commun.*, 1988, 485–486.

47 J. B. Vincent, J. C. Huffman, G. Christou, Q. Li, M. A. Nanny, D. N. Hendrickson, R. H. Fong and R. H. Fish, *J. Am. Chem. Soc.*, 1988, **110**, 6898–6900.
48 W. Nam and J. S. Valentine, *New J. Chem.*, 1989, **13**, 677–682.
49 R. A. Leising, R. E. Norman and L. Que Jr., *Inorg. Chem.*, 1990, **29**, 2553–2555.
50 R. H. Fish, M. S. Konings, K. J. Oberhausen, R. H. Fong, W. M. Yu, G. Christou, J. B. Vincent, D. K. Coggin and R. M. Buchanan, *Inorg. Chem.*, 1991, **30**, 3002–3006.
51 H. C. Tung, C. Kang and D. T. Sawyer, *J. Am. Chem. Soc.*, 1992, **114**, 3445–3455.
52 D. H. R. Barton and D. Doller, *Acc. Chem. Res.*, 1992, **25**, 504–512.
53 R. A. Leising, J. Kim, M. A. Perez and L. Que Jr., *J. Am. Chem. Soc.*, 1993, **115**, 9524–9530.
54 R. M. Buchanan, S. Chen, J. F. Richardson, M. Bressan, L. Forti, A. Morvillo and R. H. Fish, *Inorg. Chem.*, 1994, **33**, 3208–3209.
55 M. Lubben, A. Meetsma, E. C. Wilkinson, B. Feringa and L. Que Jr., *Angew. Chem., Int. Ed. Engl.*, 1995, **34**, 1512–1514.
56 I. W. C. E. Arends, K. U. Ingold and D. D. M. Wayner, *J. Am. Chem. Soc.*, 1995, **117**, 4710–4711.
57 S. Ito, M. Suzuki, T. Kobayashi, H. Itoh, A. Harada, S. Ohba and Y. Nishida, *J. Chem. Soc., Dalton Trans.*, 1996, 2579–2580.
58 B. Singh, J. R. Long, G. C. Papaefthymiou and P. Stavropoulos, *J. Am. Chem. Soc.*, 1996, **118**, 5824–5825.
59 C. Nguyen, R. J. Guajardo and P. K. Mascharak, *Inorg. Chem.*, 1996, **35**, 6273–6281.
60 M. Kodera, H. Shimakoshi and K. Kano, *Chem. Commun.*, 1996, 1737–1738.
61 S. Mukerjee, A. Stassinopoulos and J. P. Caradonna, *J. Am. Chem. Soc.*, 1997, **119**, 8097–8098.
62 P. A. MacFaul, K. U. Ingold, D. D. M. Wayner and L. Que Jr., *J. Am. Chem. Soc.*, 1997, **119**, 10594–10598.
63 C. Kim, K. Chen, J. Kim and L. Que Jr., *J. Am. Chem. Soc.*, 1997, **119**, 5964–5965.
64 S. P. de Visser, J. U. Rohde, Y. M. Lee, J. Cho and W. Nam, *Coord. Chem. Rev.*, 2013, **257**, 381–393.
65 S. P. de Visser, L. Tahsini and W. Nam, *Chem. – Eur. J.*, 2009, **15**, 5577–5587.
66 R. Latifi, M. Bagherzadeh and S. P. de Visser, *Chem. – Eur. J*, 2009, **15**, 6651–6662.
67 L. Tahsini, M. Bagherzadeh, W. Nam and S. P. de Visser, *Inorg. Chem.*, 2009, **48**, 6661–6669.
68 W. Nam, *Acc. Chem. Res.*, 2007, **40**, 522–531.
69 P. Comba and G. Rajaraman, *Inorg. Chem.*, 2007, **47**, 78–93.
70 E. I. Solomon, T. C. Brunold, M. I. Davis, J. N. Kemsley, S. K. Lee, N. Lehnert, F. Neese, A. J. Skulan, Y. S. Yang and J. Zhou, *Chem. Rev.*, 2000, **100**, 235–349.
71 A. Decker and E. I. Solomon, *Angew. Chem., Int. Ed.*, 2005, **44**, 2252–2255.
72 F. Neese, *J. Inorg. Biochem.*, 2006, **100**, 716–726.
73 A. Ghosh, E. Tangen, H. Ryeng and P. R. Taylor, *Eur. J. Inorg. Chem.*, 2004, 4555–4560.
74 D. Kumar, H. Hirao, L. Que Jr. and S. Shaik, *J. Am. Chem. Soc.*, 2005, **127**, 8026–8027.
75 T. Kamachi, T. Kouno, W. Nam and K. Yoshizawa, *J. Inorg. Biochem.*, 2006, **100**, 751–754.
76 S. P. de Visser, *Angew. Chem., Int. Ed.*, 2006, **45**, 1790–1793.
77 O. Pestovsky, S. Stoian, E. L. Bominaar, X. Shan, E. Münck, L. Que Jr. and A. Bakac, *Angew. Chem., Int. Ed.*, 2005, **117**, 6871–6874.
78 A. E. Anastasi, P. Comba, J. McGrady, A. Lienke and H. Rohwer, *Inorg. Chem.*, 2007, **46**, 6420–6426.
79 A. Dey and A. Ghosh, *J. Am. Chem. Soc.*, 2002, **124**, 3206–3207.
80 J. T. Groves, Z. Gross and M. K. Stern, *Inorg. Chem.*, 1994, **33**, 5065–5072.
81 T. A. van den Berg, J. W. de Boer, W. R. Browne, G. Roelfes and B. L. Feringa, *Chem. Commun.*, 2004, 2550–2551.
82 P. M. Kozlowski, J. Kuta, T. Ohta and T. Kitagawa, *J. Inorg. Biochem.*, 2006, **100**, 744–750.
83 J. Terner, V. Palaniappan, A. Gold, R. Weiss, M. M. Fitzgerald, A. M. Sullivan and C. M. Hosten, *J. Inorg. Biochem.*, 2006, **100**, 480–501.
84 C. A. Grapperhaus, B. Mienert, E. Bill, T. Weyhermüller and K. Wieghardt, *Inorg. Chem.*, 2000, **39**, 5306–5317.
85 A. Decker, J.-U. Rohde, L. Que Jr. and E. I. Solomon, *J. Am. Chem. Soc.*, 2004, **126**, 5378–5379.
86 M. P. Jensen, S. J. Lange, M. P. Mehn, E. L. Que and L. Que Jr., *J. Am. Chem. Soc.*, 2003, **125**, 2113–2128.
87 F. Aquino and J. H. Rodriguez, *J. Chem. Phys.*, 2005, **123**, 204902–204906.
88 C. V. Sastri, M. J. Park, T. Ohta, T. A. Jackson, A. Stubna, M. S. Seo, J. Lee, J. Kim, T. Kitagawa, E. Munck, L. Que Jr. and W. Nam, *J. Am. Chem. Soc.*, 2005, **127**, 12494–12495.
89 D. Wang, K. Ray, M. J. Collins, E. R. Farquhar, J. R. Frisch, L. Gomez, T. A. Jackson, M. Kerscher, A. Waleska, P. Comba, M. Costas and L. Que Jr., *Chem. Sci.*, 2013, **4**, 282–291.
90 I. Prat, J. S. Mathieson, M. Guell, X. Ribas, J. M. Luis, L. Cronin and M. Costas, *Nat. Chem.*, 2011, **3**, 788–793.
91 F. T. de Oliveira, A. Chanda, D. Banerjee, X. P. Shan, S. Mondal, L. Que Jr., E. L. Bominaar, E. Munck and T. J. Collins, *Science*, 2007, **315**, 835–838.
92 K. M. Van Heuvelen, A. T. Fiedler, X. P. Shan, R. F. De Hont, K. K. Meier, E. L. Bominaar, E. Munck and L. Que Jr., *Proc. Natl. Acad. Sci. U. S. A.*, 2012, **109**, 11933–11938.
93 O. Y. Lyakin, K. P. Bryliakov, G. J. P. Britovsek and E. P. Talsi, *J. Am. Chem. Soc.*, 2009, **131**, 10798–10799.
94 A. Ansari, A. Kaushik and G. Rajaraman, *J. Am. Chem. Soc.*, 2013, **135**, 4235–4249.
95 S. Taktak, M. Flook, B. M. Foxman, L. Que Jr. and E. V. Rybak-Akimova, *Chem. Commun.*, 2005, 5301–5303.
96 K. Chen and L. Que Jr., *Chem. Commun.*, 1999, 1375–1376.
97 M. Costas, A. K. Tipton, K. Chen, D.-H. Jo and L. Que Jr., *J. Am. Chem. Soc.*, 2001, **123**, 6722–6723.
98 M. Costas, K. Chen and L. Que Jr., *Coord. Chem. Rev.*, 2000, **200**, 517–544.
99 M. C. White, A. G. Doyle and E. N. Jacobsen, *J. Am. Chem. Soc.*, 2001, **123**, 7194–7195.

100 J. Y. Ryu, J. Kim, M. Costas, K. Chen, W. Nam and L. Que Jr., *Chem. Commun.*, 2002, 1288–1289.
101 W. N. Oloo, A. J. Fielding and L. Que Jr., *J. Am. Chem. Soc.*, 2013, **135**, 6438–6441.
102 L. V. Liu, S. Hong, J. Cho, W. Nam and E. I. Solomon, *J. Am. Chem. Soc.*, 2013, **135**, 3286–3299.
103 A. Thibon, V. Jollet, C. Ribal, K. Senechal-David, L. Billon, A. B. Sorokin and F. Banse, *Chem. – Eur. J.*, 2012, **18**, 2715–2724.
104 M. J. Frisch and *et al.*, *Gaussian 09, revision 02*, Gaussian, Inc., Wallingford, CT, 2009.
105 A. D. Becke, *J. Chem. Phys.*, 1993, **98**, 5648–5652.
106 C. Lee, W. Yang and R. G. Parr, *Phys. Rev. B: Condens. Matter Mater. Phys.*, 1988, **37**, 785–789.
107 S. Grimme, *Comput. Chem.*, 2006, **27**, 1787.
108 J. D. Chai and M. Head-Gordon, *Phys. Chem. Chem. Phys.*, 2008, **10**, 6615–6620.
109 Y. Zhao and D. G. Truhlar, *Theor. Chem. Acc.*, 2008, **120**, 215–241.
110 N. C. Handy and A. Cohen, *J. Mol. Phys.*, 2001, **99**, 401–413.
111 J. M. Tao, J. P. Perdew, V. N. Staroverov and G. E. Scuseria, *Phys. Rev. Lett.*, 2003, **91**, 146401.
112 C. Møller and M. S. Plesset, *Phys. Rev.*, 1934, **46**, 618–622.
113 M. Jaccob, A. Ansari, B. Pandey and G. Rajaraman, *Dalton Trans.*, 2013, **42**, 16518–16526.
114 H. Hirao, D. Kumar, L. Que Jr. and S. Shaik, *J. Am. Chem. Soc.*, 2006, **128**, 8590–8606.
115 H. Hiro, D. Kumar, W. Thiel and S. Shaik, *J. Am. Chem. Soc.*, 2005, **127**, 13007–13018.
116 C. M. Bathelt, J. Zurek, A. J. Mulholland and J. N. Harvey, *J. Am. Chem. Soc.*, 2005, **127**, 12900–12908.
117 A. Bassan, M. R. A. Blomberg, P. E. M. Siegbahn and L. Que Jr., *Angew. Chem., Int. Ed.*, 2005, **44**, 2939–2941.
118 P. E. M. Siegbahn, *J. Biol. Inorg. Chem.*, 2006, **11**, 695–701.
119 P. E. M. Siegbahn and T. Borowski, *Acc. Chem. Res.*, 2006, **39**, 729–738.
120 A. Ghosh, *J. Biol. Inorg. Chem.*, 2006, **11**, 671–673.
121 A. Ghosh, *J. Biol. Inorg. Chem.*, 2006, **11**, 712–724.
122 F. Neese, *J. Biol. Inorg. Chem.*, 2006, **11**, 702–711.
123 L. Noodleman and W. G. Han, *JBIC, J. Biol. Inorg. Chem.*, 2006, **11**, 674–694.
124 E. Olsson, A. Martinez, K. Teigen and V. R. Jensen, *Chem. – Eur. J.*, 2011, **17**, 3746–3758.
125 E. Olsson, A. Mertinez, K. Teigen and V. R. Jensen, *Eur. J. Inorg. Chem.*, 2011, 2720–2732.
126 K. P. Kepp, *J. Inorg. Biochem.*, 2011, **105**, 1286–1292.
127 T. H. J. Dunning and P. J. Hay, in *Modern Theoretical Chemistry*, ed. H. F. Schaefer, III, Plenum, New York, 1976, vol. 3, p. 1.
128 P. J. Hay and W. R. Wadt, *J. Chem. Phys.*, 1985, **82**, 270–283.
129 P. J. Hay and W. R. Wadt, *J. Chem. Phys.*, 1985, **82**, 299–310.
130 W. R. Wadt and P. J. Hay, *J. Chem. Phys.*, 1985, **82**, 284–298.
131 R. Ditchfield, W. J. Hehre and J. A. Pople, *J. Chem. Phys.*, 1971, **54**, 724–728.
132 A. Schaefer, H. Horn and R. Ahlrichs, *J. Chem. Phys.*, 1992, **97**, 2571–2577.
133 C. Schaefer, C. Huber and R. Ahlrichs, *Chem. Phys.*, 1994, **100**, 5829–5835.
134 P. Fluckiger, H. P. Luthi, S. Portmann and J. Weber, *Molekel 4.3*, Swiss Center for Scientific Computing, Manno, Switzerland, 2000.
135 S. Portmann and H. P. Luthi, *Chimia*, 2000, **54**, 766–770.
136 A. Mairata i Payeras, R. Y. N. Ho, M. Fujita and L. Que Jr., *Chem. – Eur. J.*, 2004, **10**, 4944–4953.
137 O. V. Makhlynets, W. N. Oloo, Y. S. Moroz, I. G. Belaya, T. D. Palluccio, A. S. Filatov, P. Muller, M. A. Cranswick, L. Que Jr. and E. V. Rybak-Akimova, *Chem. Commun.*, 2014, **50**, 645–648.
138 S. F. Ye and F. Neese, *Inorg. Chem.*, 2010, **49**, 772–774.
139 M. Schmidt, D. Wiedemann, B. Moubaraki, N. F. Chilton, K. S. Murray, K. R. Vignesh, G. Rajaraman and A. Grohmann, *Eur. J. Inorg. Chem.*, 2013, 958–967.
140 J. N. Harvey, M. Aschi, H. Schwarz and W. Koch, *Theor. Chem. Acc.*, 1998, **99**, 95–99.
141 M. H. Lim, J.-U. Rohde, A. Stubna, M. R. Bukowski, M. Costas, R. Y. N. Ho, E. Munck, W. Nam and L. Que Jr., *Proc. Natl. Acad. Sci. U. S. A.*, 2003, **100**, 3665–3670.
142 J.-U. Rohde, A. Stubna, E. L. Bominaar, E. Munck, W. Nam and L. Que, *Inorg. Chem.*, 2006, **45**, 6435–6445.
143 M. S. Seo, N. H. Kim, K.-B. Cho, J. E. So, S. K. Park, M. Clemancey, R. Garcia-Serres, J.-M. Latour, S. Shaik and W. Nam, *Chem. Sci.*, 2011, **2**, 1039–1045.
144 A. Bassan, M. R. A. Blomberg, P. E. M. Siegbahn and L. Que Jr., *J. Am. Chem. Soc.*, 2002, **124**, 11056–11063.
145 A. R. McDonald and L. Que Jr., *Coord. Chem. Rev.*, 2013, **257**, 414–428.
146 S. D. Wong, C. B. Bell III, L. V. Liu, Y. Kwak, J. England, E. E. Alp, J. Zhao, L. Que Jr. and E. I. Solomon, *Angew. Chem., Int. Ed.*, 2011, 3215–3218.
147 K. B. Cho, S. Shaik and W. Nam, *Chem. Commun.*, 2010, **46**, 4511–4513.
148 J. England, M. Martinho, E. R. Farquhar, J. R. Frisch, E. L. Bominaar, E. Munck and L. Que Jr., *Angew. Chem., Int. Ed.*, 2009, **48**, 3622–3626.
149 D. C. Lacy, R. Gupta, K. L. Stone, J. Greaves, J. W. Ziller, M. P. Hendrich and A. S. Borovik, *J. Am. Chem. Soc.*, 2010, **132**, 12188–12190.
150 K. L. Kostka, B. G. Fox, M. P. Hendrich, T. J. Collins, C. E. F. Rickard, L. J. Wright and E. Munck, *J. Am. Chem. Soc.*, 1993, **115**, 6746–6757.
151 P. Pestovsky, S. Stoian, E. L. Bominaar, X. Shan, E. Munck, L. Que Jr. and A. Bakac, *Angew. Chem., Int. Ed.*, 2005, **44**, 6871–6874.
152 We are unable to obtain ^{4}II-2$_{hs}$ and ^{2}II-2$_{is}$ species due to SCF convergence issue.
153 J. Bautz, P. Comba, C. L. de Laorden, M. Menzel and G. Rajaraman, *Angew. Chem., Int. Ed.*, 2007, **46**, 8067–8070.
154 P. Comba, G. Rajaraman and H. Rohwer, *Inorg. Chem.*, 2007, **46**, 3826–3838.